Available online at www.rsu.ac.th/rjas

Rangsit Journal of Arts and Sciences, January-June 2015 RJAS Vol. 5 No. 1, pp. 49-62

ISSN 2229-063X (Print)/ISSN 2392-554X (Online)

Effect of modified expansion pipe nozzle on heat transfer enhancement with impinging jet

Natthaporn Kaewchoothong, Makatar Wae-hayee, Passakorn Vessakosol, and Chayut Nuntadusit*

Department of Mechanical Engineering, Faculty of Engineering, Prince of Songkla University,
Hatyai, Songkhla, 90112, Thailand
E-mail: chayut@me.psu.ac.th

*Corresponding author

Submitted 26 December 2014; accepted in final form 17 April 2015
Available online 15 June 2015

Abstract

The aim of this study is to experimentally and numerically investigate the flow and heat transfer characteristics of impinging jet from expansion pipe with some modifications. The expansion pipe without air entrainment hole, with 4 and 8 air entrainment holes and hollow expansion pipe were connected to pipe nozzle and assessed to obtain the condition of heat transfer augmentation. The results from cases with expansion pipe were compared with cases of conventional pipe (without expansion pipe). In this study, the inner diameters of main pipe and expansion pipe were d=17.2 mm and D=68.8 mm (i.e., D=4d), respectively. The jet-to-plate distance (the distance from main pipe outlet to impingement surface) was varied at H=4d, 6d and 8d. The length of expansion pipe was fixed at L=2d, 4d and 6d. The comparison of all results was based on constant jet mass flow rate with Reynolds number of jet from the main pipe nozzle at Re=20,000. An infrared camera was used to measure the temperature distribution on the impingement surface, and the measured data were subsequently evaluated to gain Nusselt number distributions on the surface. The 3-D numerical simulation with SST k-ω turbulence model was carried out to investigate the flow field. The results show that the amount of ambient air entrained to the hollow expansion pipe is larger than the case of expansion pipe with air entrainment holes. Consequently, the heat transfer on the impingement surface for the case of hollow expansion pipe can be enhanced massively, especially for case of L=2d at H=4d.

Keywords: *impinging jet, expansion pipe nozzle, air entrainment, heat transfer enhancement*

บทคัดย่อ

จุดประสงค์ของงานวิจัยเพื่อศึกษาลักษณะการไหลและการถ่ายเทความร้อนของเจ็ทพุ่งชนจากท่อขยายหน้าตัดที่มีการปรับแต่งโดยใช้วิธีทดลองและจำลองการไหลเชิงตัวเลข ท่อขยายหน้าตัดแบบไม่เจาะรูเหนี่ยวนำอากาศ, แบบเจาะรูเพื่อเพิ่มการเหนี่ยวนำอากาศ 4 รูและ 8 รู และแบบท่อกลวงถูกนำมาติดตั้งหน้าท่อเจ็ท เพื่อพิจารณาหาเงื่อนไขที่สามารถเพิ่มการถ่ายเทความร้อนได้ และผลของการติดตั้งท่อขยายหน้าตัดทั้งหมดถูกนำมาเปรียบเทียบกับกรณีเจ็ทจากท่อปกติ (ไม่มีการติดตั้งท่อขยายหน้าตัด) ในการทดลองได้กำหนดขนาดเส้นผ่าศูนย์กลางภายในของท่อเจ็ทและท่อขยายหน้าตัดที่ d=17.2 มม และ D=68.8 มม (=4d) ตามลำดับ ระยะจากปากทางออกเจ็ทถึงพื้นผิวที่เจ็ทพุ่งชน (ระยะจากปากทางออกของท่อหลักถึงพื้นผิวที่เจ็ทพุ่งชน) ถูกเปลี่ยนที่ H=4d, 6d และ 8d และความยาวท่อขยายหน้าตัดถูกกำหนดที่ L=2d, 4d และ 6d ในการเปรียบเทียบผลการทดลองกำหนดให้อัตราการไหลของเจ็ทเท่ากันทุกกรณีโดยเทียบจากค่าเรย์โนลดส์นัมเบอร์ของเจ็ทจากท่อปกติที่ Re=20,000 สำหรับวิธีการทดลองได้ใช้กล้องอินฟราเรดวัดการกระจายอุณหภูมิบนพื้นผิวที่เจ็ทพุ่งชนและคำนวณหาการกระจายนัสเซิลต์นัมเบอร์บนพื้นผิว สำหรับการศึกษาลักษณะการไหลของเจ็ทพุ่งชนได้สร้างแบบจำลองเชิงตัวเลข 3 มิติ และใช้โมเดลการไหลแบบปั่นป่วนแบบ SST k-ω ในการจำลองการไหล จากผลการศึกษาพบว่าปริมาณของอากาศที่อยู่รอบๆถูกเหนี่ยวนำเข้าสู่ท่อขยายหน้าตัดแบบกลวงมากกว่ากรณีท่อขยายหน้าตัดแบบเจาะรูเหนี่ยวนำอากาศ จึงส่งผลให้การถ่ายเทความร้อนบนพื้นผิวของเจ็ทจากท่อขยายหน้าตัดแบบกลวงเพิ่มขึ้นอย่างเห็นได้ชัด โดยเฉพาะในกรณีที่ L=2d ที่ H=4d

คำสำคัญ: *เจ็ทพุ่งชน, หัวฉีดแบบท่อขยาย, การเหนี่ยวนำอากาศ, การเพิ่มการถ่ายเทความร้อน*

1. Introduction

Impinging jet or jet impingement is a heat transfer augmentation technique using fluid of the jet flow directly impinging on a heat transfer surface. It has wide applications for cooling or heating on the surface of thermal equipment in industrial applications, such as tempering of glass, drying of paper, thermal exchanging in heat exchanger of solar air heater, cooling in electronic components and more specifically in turbine

blades. The heat transfer rate is very high in the jet impingement region then decreases gradually along the wall leaving the impingement region (Viskanta, 1993). The characteristics of heat transfer depend on the flow structure of the jet before impingement (Rohlfs, Haustein, Garbrecht, & Kneer, 2012). So, flow control of impinging jet is very important key to enhance heat transfer on the impingement surface.

Many researchers have extensively studied flow and heat transfer characteristics of the impinging jet. Ashforth-Frost and Jambunathan (1996) reported the flow characteristics of the jet where the decaying of axial velocity coincides with the increasing of axial turbulent intensity. The jet potential core defined as the distance from the nozzle outlet to where the axial velocity decreased to 95% of the initial axial velocity was found between 4.5d-5.8d (where d is nozzle diameter) depending on nozzle geometry. Ashforth-Frost, Jambunathan, and Whitney (1997) studied flow and heat transfer characteristics on a surface of the impinging jet. They reported that the increasing of heat transfer on an impingement surface is from two factors: axial jet momentum impinging on the target surface and turbulent intensity of the jet before impingement. Zhou and Lee (2004) tried to increase heat transfer on the impingement surface by adding mesh screen at the jet outlet to increase turbulent flow. The results show that the heat transfer on the impingement surface was higher than the case of a conventional jet in the jet-to-plate distance of $H \geq 4d$ due to higher turbulent intensity. However, when the jet-to-plate distance is outside of this range, the conventional jet was better than the addition of the mesh screen. Moreover, there are several methods to increase heat transfer on an impingement surface by modifying the jet outlet to increase turbulent intensity in jet flow such as inserting twisted tape (Nuntadusit, Wae-hayee, Bunyajitradulya, & Eiamsa-ard, 2012), adding guide vanes (Huang & El-Genk, 1998) into pipe nozzles, attaching triangular tabs at jet outlets (Gao, Sun, & Ewing, 2003), and using lobed nozzles (Martin & Buchlin, 2011).

Many researchers reported that an expanding of the jet outlet can increase the entrainment of ambient fluid into the jet flow (Hasan & Hussain, 1982; Selerowicz, Szumowski, & Meier, 1991; Zeng, New, & Tsai, 2009; Zeng, New, & Chng, 2011). A simple method to increase jet entrainment is to expand the nozzle outlet. Due to low pressure occurring inside the expansion pipe (with respect to atmosphere pressure), the ambient fluid was induced to enter and to mix with jet flow inside the expansion pipe. The amount of induced ambient fluid of expansion pipe is more than the conventional jet. Consequently, the turbulent intensity inside the jet flow for the expansion pipe is relatively higher than the conventional pipe. Usually, the expansion pipe is used for enhancing jet mixing or combustion in industrial applications (Nathan, Hill, & Luxton, 1998; Nathan, Alwahabi, Newbold, & Nobes, 2006). However, there are no concerns to enhance the heat transfer on impingement surfaces by using an expansion pipe.

2. Objectives

The goal of this paper is to apply the expansion pipe on jet impingement for enhancing the heat transfer on impingement surface. Moreover, from previous work, the entrainment of ambient air into the jet flow occurs only around the edge of the expansion pipe. So, objective of this work is also to enhance the entrainment air by using an expansion pipe with air entrainment holes and a hollow expansion pipe. The entrainment air might move more air through modified expansion pipes and might increase turbulent intensity of the impinging jet resulting in increased heat transfer on the impingement surface.

The secondary aim of this study is to investigate the flow and heat transfer characteristics of the impinging jet from an expansion pipe with and without entrainment holes as well as a hollow expansion pipe. The effect of expansion pipe geometry was experimentally and numerically investigated. The effect of jet-to-plate distance was also examined. The comparison of the results is based on constant jet mass flow rate. The temperature distributions on the impingement surface were measured using an infrared camera, and flow characteristics of impinging jet were revealed by using Computational Fluid Dynamic (CFD) technique.

3. Experimental set-up and method

3.1 Experimental model and parameters

The experimental model of the impinging jet from the expansion pipe with air entrainment holes and hollow expansion pipe are shown in Figure 1(a) and 1(b), respectively. The jet was

discharged from the pipe nozzle and perpendicularly impinged on a flat wall. The expansion pipe with different geometries was assembled at the end of the main pipe nozzle. An origin of the Cartesian coordinates was located at the centre of the expansion pipe outlet. The Z-axis is on the axial of the jet, and X-, Y-axes are normal to the axial of the jet in the horizontal and vertical directions, respectively.

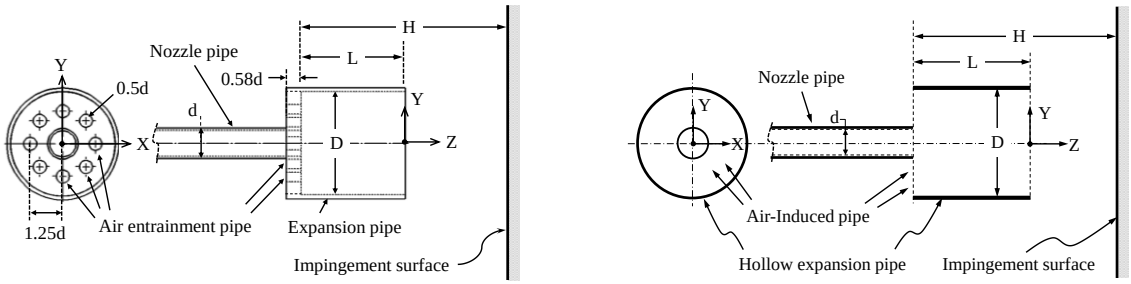

(a) Expansion pipe with air entrainment holes (b) Hollow expansion pipe

Figure 1 Experimental model of impinging jet from expansion pipe

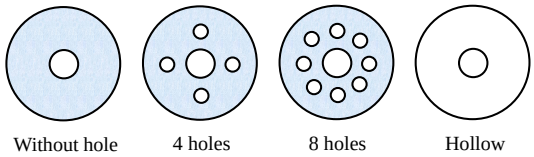

Figure 2 Geometry of expansion pipe without hole, with 4 and 8 air entrainment holes, and hollow expansion pipe

For all experiments, the Reynolds number of jet flow was fixed at Re=20,000 (based on inner diameter of main pipe and jet velocity at the center of the pipe nozzle). The conventional impinging jet from the pipe nozzle was also examined for comparison with the expansion pipe.

Some of the modified expansion pipes examined without air entrainment holes, with 4 and 8 air entrainment holes and hollow expansion pipe are shown in Figure 2. The jet-to-plate distance (the distance from the main pipe outlet to the impingement surface) was varied at H=4d, 6d and 8d where d is inner diameter of main pipe at 17.2 mm. The inner diameter of the expansion pipe was fixed at D=4d whereas the expansion pipe lengths were varied at L=2d, 4d and 6d.

The expansion pipe was assembled at the end of the main pipe with concentric holes. The expansion pipes with air entrainment holes were opened on the expansion wall. The diameter of each air entrainment hole was 0.5d and each hole located at 1.25d from the center of the expansion pipe (see details in Figure 1(a)). The hollow expansion pipe was handled independently with the main pipe nozzle. The expansion pipe was connected with a movable and controllable arm and carefully positioned to be concentric with the main pipe.

3.2 Experimental setup

The experimental setup is shown in Figure 3. A 1-HP blower accelerated the air which then flowed through an orifice flow meter and temperature controlled chamber equipped with 2-kW heater. Jet air temperature was controlled by a temperature controller and a power controller at 27±0.2°C. The jet flow rate was controlled by adjusting the rotating speed of the blower with an inverter. The turbulent jet flow is discharged from the round pipe with an inner diameter of d=17.2 mm and length of 83D. This pipe length is ensured fully developed flow at Re=20,000. Two layers of mesh plate were mounted at the entrance of the pipe to ensure the jet temperature was uniform.

The target plate made of plastic plate (460 mm×460 mm and 10 mm thick) was opened to square window at its center. A stainless steel foil (240 mm×240 mm, 0.03 mm thick) was tightly stretched between two copper bus bars over the square window on the target plate. This stainless steel foil was used as a heat transfer surface for the jet impingement. An infrared camera (Testo 882) captured the temperature distribution on the rear side of the jet impingement surface. The temperature on the impingement surface and the camera surface were considered the same because the stainless steel foil is sufficiently thin. The impingement surface was movable in the Z-axis direction for adjusting the required jet-to-plate distance.

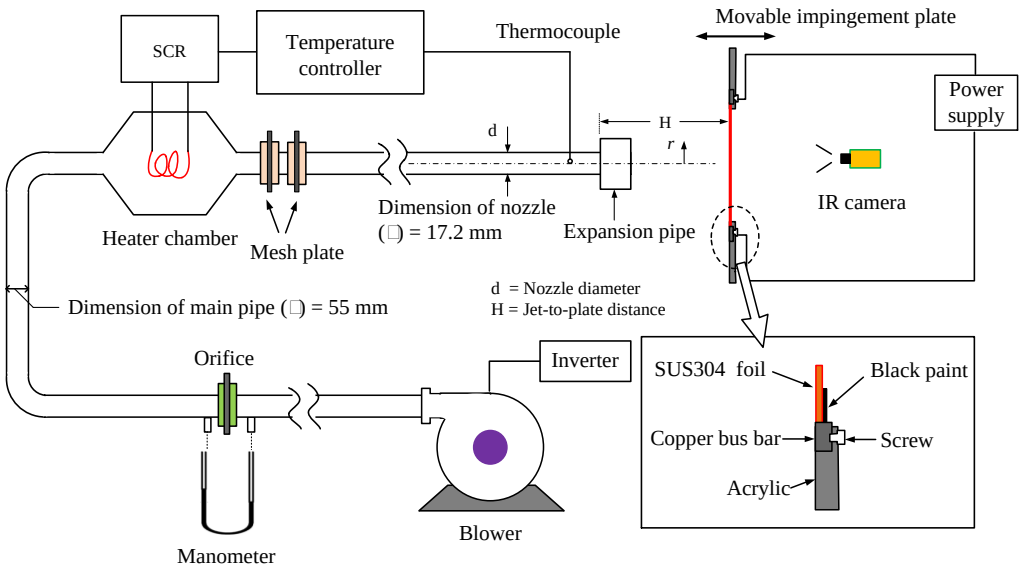

Figure 3 Layout of experimental setup

3.3 Data reduction

The impingement surface was heated by a DC power supply during the experiment. The heat dissipated uniformly on the surface and can be considered a constant heat flux condition. The input energy can be evaluated from

$$\dot{q}_{input} = \frac{IV}{A} \qquad (1)$$

, where I is the electric current, V and A are the voltage cross the copper bus bars and the area of the stainless steel foil, respectively.

The heated impingement surface was then cooled by impinging jet near room temperature. The local heat transfer coefficient and Nusselt number were then calculated from:

$$h = \frac{\dot{q}_{input} - \dot{q}_r - \dot{q}_c}{T_w - T_{aw}} \qquad (2)$$

$$Nu = \frac{hd}{k} \qquad (3)$$

where $\dot{q}_r = \sigma\varepsilon\left(\bar{T}_w^4 - T_s^4\right)$ and $\dot{q}_c = h_c(\bar{T}_w - T_s)$ are the heat losses to the environment by radiation and natural convection from the rear side of the impingement surface, respectively; T_w is the wall temperature with heat flux when cooled by the impinging jet; T_{aw} is the wall temperature without heat flux when impinged by impinging jet; σ is the Stefan-Boltzman constant; ε is the emissive coefficient of captured side; T_s is the surrounding temperature; and h_c is the natural heat transfer coefficient calculated from natural convective heat transfer from the heat transfer surface to the surrounding and k is a thermal conductivity of the air jet.

An uncertainty of heat transfer measurement was evaluated using the calculation method suggested by Kline and McClintock

RJAS Vol. 5 No. 1 Jan.-Jun. 2015, pp. 49-62
ISSN 2229-063X (Print)/ISSN 2392-554X (Online)

(1953). The uncertainty of Nusselt number was between 2.61% and 4.63%. This range was almost the same as previous works (Katti & Prabhu, 2008; Wae-Hayee, Tekasakul, Eiamsa-ard, & Nuntadusit, 2015).

3.4 Numerical model and procedure

The 3-D numerical domain is shown in Figure 4. The commercial package ANSYS ver.13.0 (Fluent) was used in this study. The numerical model was the same with the experimental model in geometries, dimensions, and jet Reynolds number. The velocity inlet was set uniformly at 14 m/s to get the Reynolds number of 20,000 at the jet nozzle outlet, and pressure outlet was set at the same atmosphere pressure. The generated grids were concentrated in the expansion pipe, near the impingement wall and mixing region as shown in Figure 5(a). It should be noted that in regard to grid dependence on impingement wall, it is very important to resolve the flow field within the viscous sublayer. To consider grid dependence on the impingement wall, y+ distributions on the impingement surface passing the jet centerline are plotted with variations of generated elements, as shown in Figure 5(b). The majority of the element variation was due to the division of the element layer above from the impingement surface. A slight discrepancy between the cases of 3,384,160 and 3,985,108 elements was detected due to the saturation of element variation on the result, and their y+ distributions were lower than 5. This element layer above the impingement plate is adequate for resolving the problems under the viscous sublayer, as mentioned by Salim, Ariff, and Cheah (2010). In this work, 3,384,160 elements were chosen for calculating the numerical problem.

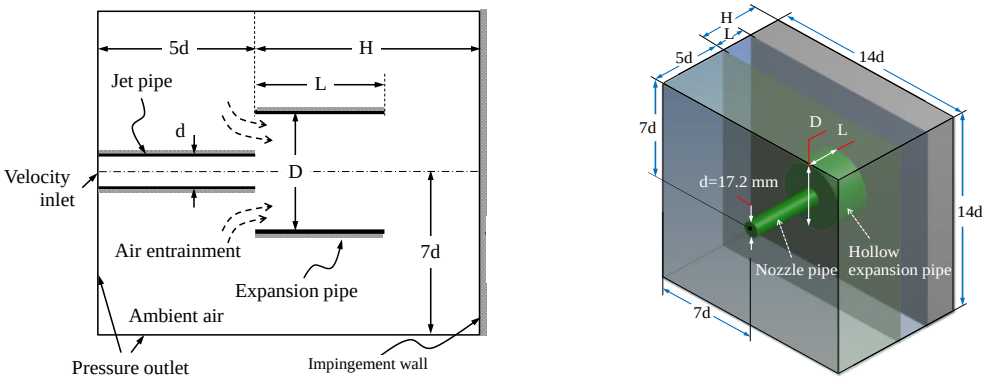

(a) 2-D Numerical domain (b) 3-D Numerical domain

Figure 4 Numerical model and boundary conditions for the case of hollow expansion pipe

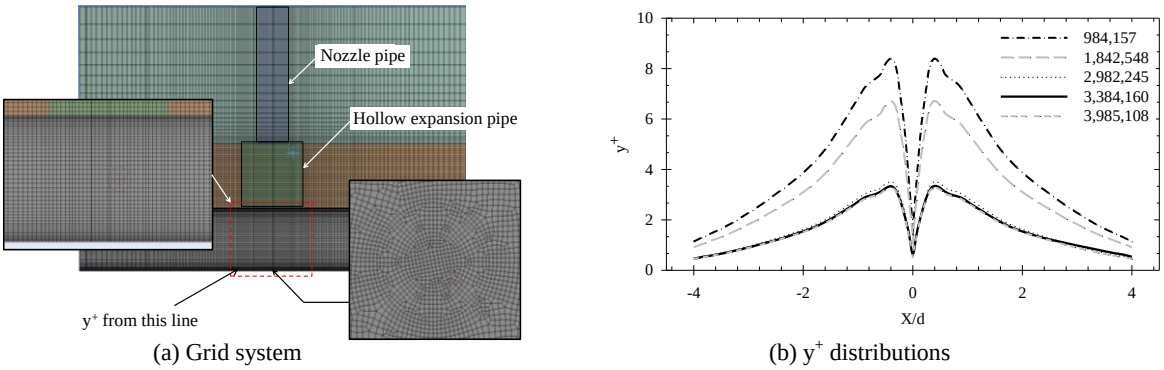

(a) Grid system (b) y^+ distributions

Figure 5 (a) Generated grid and (b) effect of grid dependence on y^+ distributions on impingement surface along jet centerline (Z/D=0) for the case of hollow expansion pipe

Computations were conducted by solving Reynolds averaged continuity and Navier-stokes equations under existing boundary conditions. The SST k-ω turbulence model was selected for this computation. This turbulence model has been adopted in solving many numerical simulations of jet impingement problems (Zuckerman & Lior, 2006; Heo, Lee, Salim, & Cheah, 2009). It has excellently predicted the solutions of impingement problems with moderate computation cost. The SIMPLE algorithm was used with second order upwind scheme for all spatial discretization. The convergence of an iterative solution has been insured when the residual of all the variables is less than the specified values. The specified value is 1×10^{-4} for continuity and momentum equations.

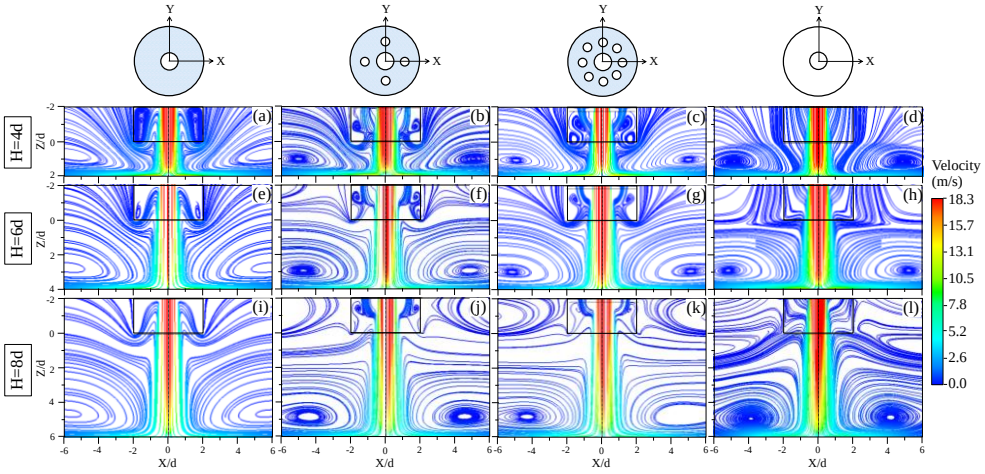

Figure 6 Streamlines of jet and ambient air on YZ plane passing the center of nozzle for the case of L=2d (CFD results, Re=20,000)

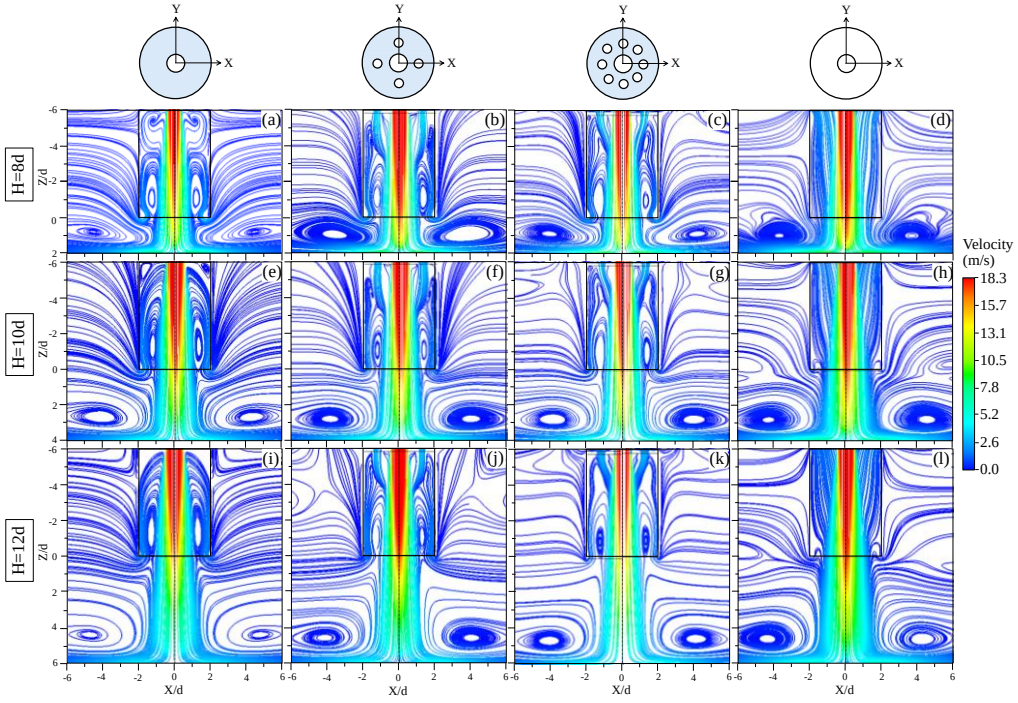

Figure 7 Streamlines of jet and ambient air on YZ plane passing the center of nozzle for the case oh L=6d (CFD results, Re=20,000)

4. Results and discussions

4.1 Flow characteristics

Streamlines of jet and ambient air on the YZ plane passing the center of the pipe nozzle for the case short expansion pipe length (L=2d) and long expansion pipe length (L=6d) are shown in Figure 6 and 7, respectively. The entrainment of ambient air into the jet flow can be categorized as either primary or secondary entrainment. In primary entrainment, the ambient air entrains into the expansion pipe, while in secondary entrainment the ambient air entrains into the air entrainment holes or into the opening bottom of a hollow expansion pipe. The large circulation flow appeared above the surface after the jet impinged on the wall. The ambient air was introduced into the circulation flow. The size of circulation flow seemed to be larger when jet-to-plate distance increases.

For the case of expansion pipe without an air entrainment hole at short expansion pipe length (L=2d) and the jet-to-plate distance of H=4d as shown in Figure 6(a). The circulation flow was found inside the expansion pipe near the edge of the expansion pipe outlet. This ambient air flowed into the expansion pipe around the jet flow. The circulation flow disappeared when the jet-to-plate distance was increased at H=6d and 8d as shown in Figure 6(e) and 6(i). However, the ambient flow was still introduced into expansion pipe around the jet flow. When the length of expansion pipe was longer (L=6d) as shown in the Figure 7(a), 7(e) and 7(f), the flow characteristics of entrainment air were almost similar to the case of L=2d. In addition, two of the circulation flows detected inside the expansion pipe near the outlet seemed to be larger.

For the case expansion pipe with 4 and 8 air entrainment holes, the flow characteristics outside the expansion pipe were similar to the case of the expansion pipe without the holes. However, the flow pattern inside the expansion pipe seems to be different. For short expansion pipes where L=2d (Figure 6(b), 6(c), 6(f), 6(g), 6(j) and 6(k)), the secondary entrainment air entered through the holes and interacted with the ambient flow from the primary entrainment air. The internal circulation flow was destroyed by the secondary entrainment air. At the same time, the secondary entrainment air was blocked by primary entrainment air at expansion pipe outlet. For long expansion pipes of L=6d (Figure 7(b), 7(c), 7(f), 7(g), 7(j) and 7(k)), the air from the entrainment holes (the secondary entrainment air) interacted with the internal circulation flow. The size of internal circulation flow becomes smaller when compared to the case of the expansion pipe without air entrainment holes due to the effect of air from entrainment holes.

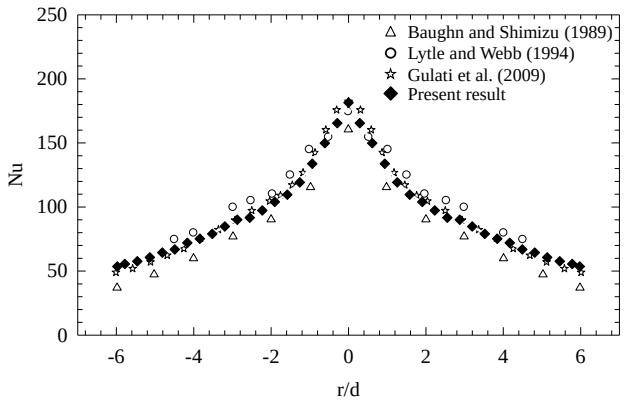

Figure 8 Comparison of Nusselt number distribution on impingement surface at jet centerline with previous works (Experiment results, *H*/*d*=6, *Re*=23,000)

For the hollow expansion pipe, the ambient air was introduced by jet flow through the hollow expansion pipe. For the short expansion pipe length L=2d at H=4d as shown in Figure 6(d), the ambient air was introduced to the hollow expansion pipe and then impinged directly on the impingement surface. This condition promoted heat transfer on the impingement surface due to high momentum of jet flow and entrainment flow impinging on the surface at low jet-to-plate distance. However, at higher jet-to-plate distances, H=6d and 8d, as shown in Figure 6(h) and 6(l), the circulation flow above the impingement surface became larger and the ambient air was introduced into the expansion pipe outlet. This results in either reducing or blocking the entrainment of ambient air in the hollow expansion pipe (the secondary entrainment air). For the long expansion pipe length, L=6d [Figure 7(d), 7(h) and 7(l)], flow characteristics were almost similar to the short expansion pipe length (L=2d). However, the contact surface between the jet and the secondary entrainment air that interact inside the hollow expansion pipe was larger due to the longer expansion pipe length. In addition, there appears to be reverse flow (ambient air flow into the expansion pipe outlet) near the edge of expansion pipe outlet at the jet-to-plate distance *H*=10d and 12d (Figure 7(h) and 7(l).

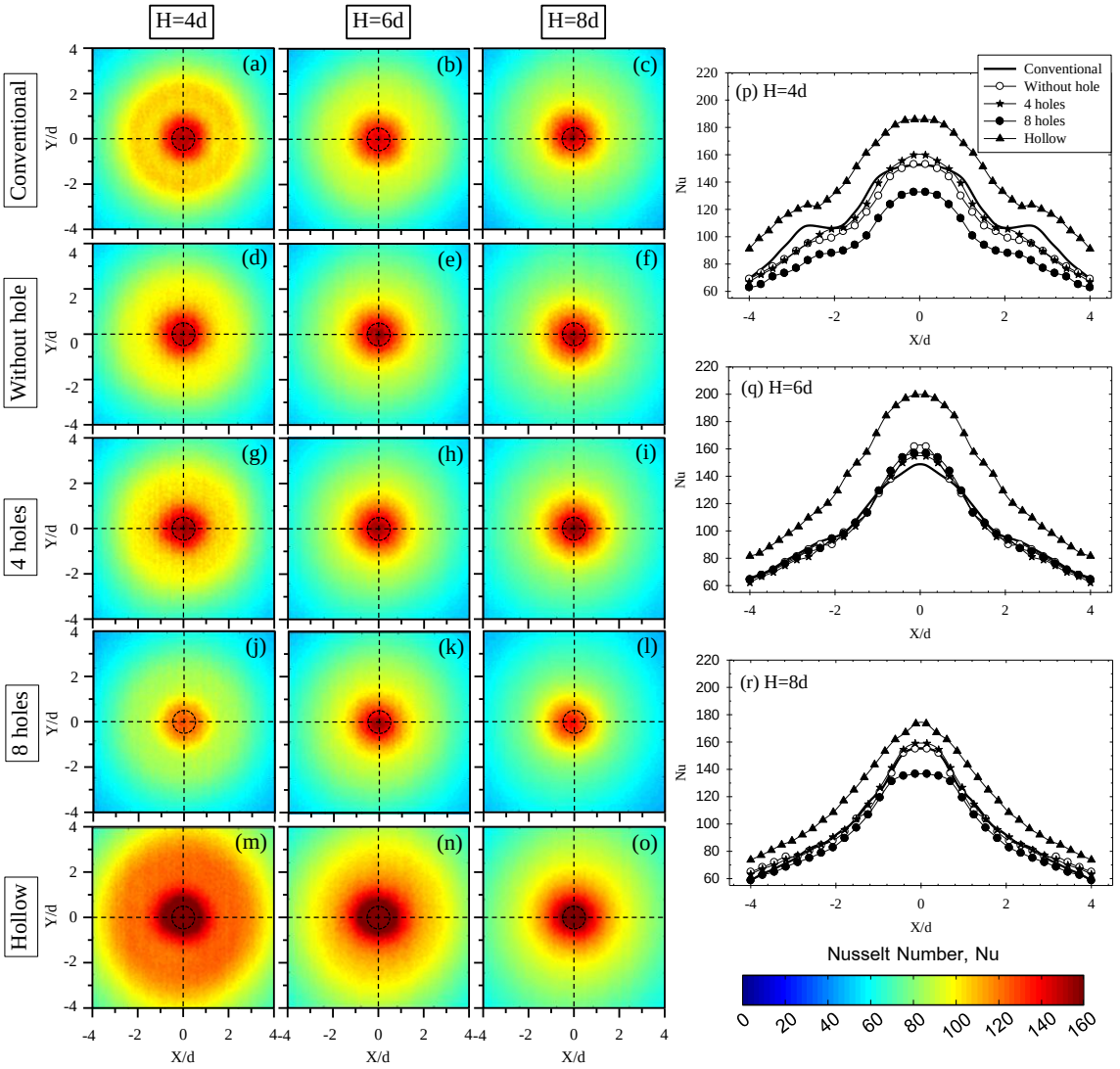

Figure 9 Nusselt number contours on impingement surface and comparison of Nusselt number distributions for the case of L=2d (Experimental result, Re=20,000)

RJAS Vol. 5 No. 1 Jan.-Jun. 2015, pp. 49-62
ISSN 2229-063X (Print)/ISSN 2392-554X (Online)

4.2 Heat transfer distributions on impingement surface

In order to verify the test section of heat transfer measurements, the Nusselt number distributions on the impingement surface at Re=23,000 and jet-to-plate distance of H=6d were compared with previous works (Baughn & Shimizu, 1989; Lytle & Webb, 1994; Gulati, Katti, & Prabhu, 2009) as shown in Figure 8. The current experimental data agree well with those in the previous work. This can be substantiated to correctly ensure the heat transfer measurements of this work.

Nusselt number contours and local Nusselt number distributions on the impingement surface for the case of expansion pipe length at L=2d, 4d and 6d are shown in Figure 9, 10 and 11, respectively. The figure in the last right column is Nusselt number distribution along the radial direction for comparison between conventional jet and jet from a nozzle with a modified expansion pipe.

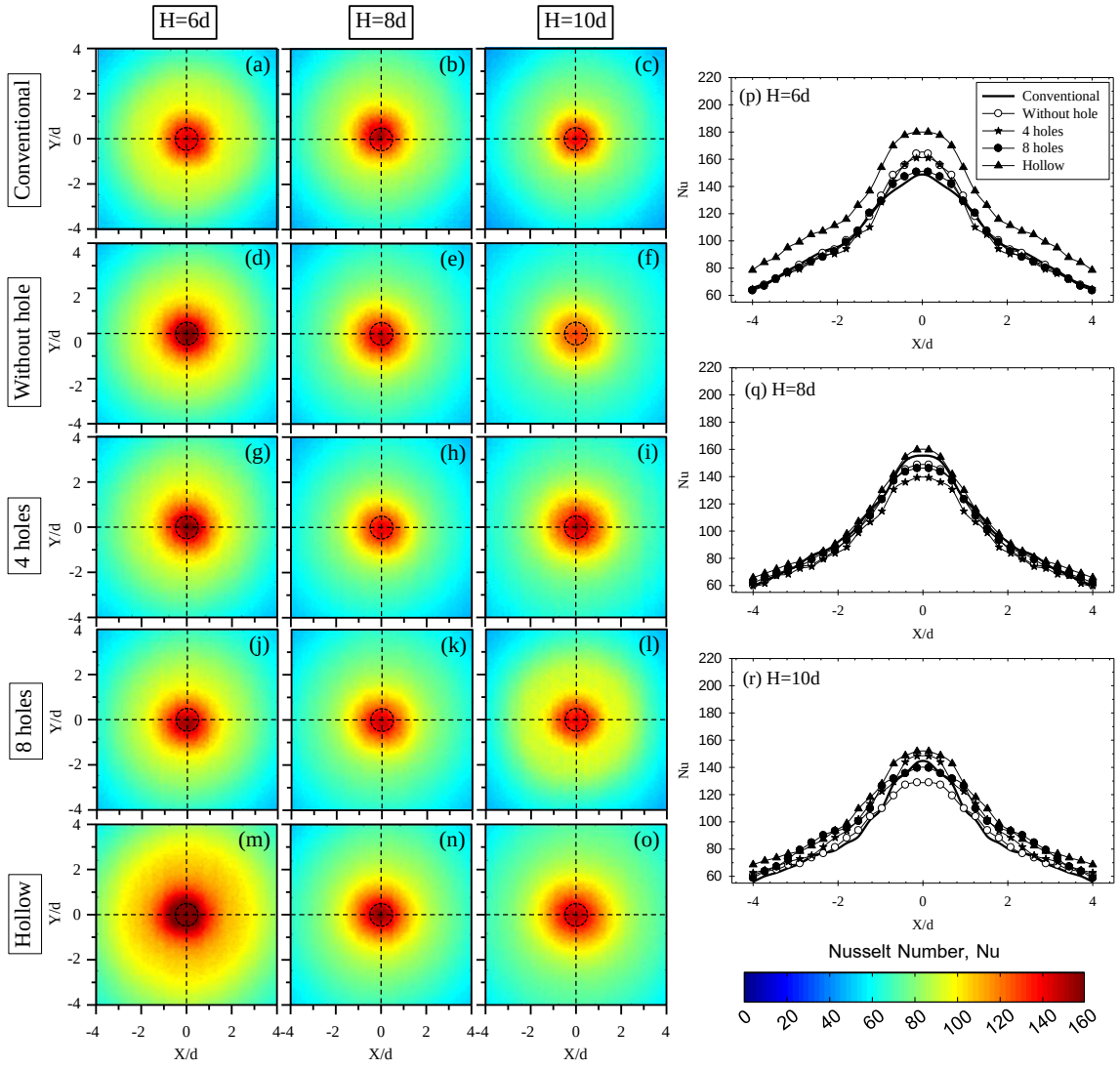

Figure 10 Nusselt number contours on impingement surface and comparison of Nusselt number distributions for the case of L=4d (Experimental result, Re=20,000)

For the case of conventional impinging jet as shown in the first line of each figure (Figure 9(a)-9(c), Figure 10(a)-10(c) and Figure 11(a)-11(c)), the Nusselt number tends to decreases according to increasing jet-to-plate distance. Nusselt number at stagnation point (X/d=0) was the highest due to high momentum and turbulence intensity along jet centerline before impingement (Ashforth-Frost & Jambunathan, 1996; Ashforth-Frost et al., 1997). The secondary peak of Nusselt number can be seen around X/d=2.5 for case of H=4d (Figure 9(p)).

For the case of the impinging jet from expansion pipe, the Nusselt number distributions tend to decrease when the jet-to-plate distance (H) becomes larger and the length of expansion pipe (L) becomes longer. The effect of increasing the jet-to-plate distance (H) on decreasing the Nusselt number was more significant than the increasing of the length of expansion pipe (L). The increasing of jet-to-plate distance (H) was more effective on changing the jet structure before impingement.

For the expansion pipe without air entrainment holes (Figure 9(d), 9(e), 9(f), Figure 10(d), 10(e), 10(f) and Figure 11(d), 11(e), 11(f)) and with 4 air entrainment holes (Figure 9(g), 9(h), 9(i), Figure 10(g), 10(h), 10(i) and Figure 11(g), 11(h), 11(i)), the Nusselt number distributions are not different when compared to the conventional pipe under the same conditions. Additionally, it can be noted that the Nusselt number at the stagnation point for both the expansion pipe without holes and with 4 air entrainment holes was slightly higher than the case of conventional pipe (observed in Figure 9(p), 9(q), 9(r), Figure 10(p), 10(q), 10(r) and Figure 11(p), 11(q), and 11(r)). Obviously, the Nusselt number distribution for the case of 8 air entrainment holes is very low as shown in Figure 9(j), 9(k), 9(l), Figure 10(j), 10(k), 10(l) and Figure 11(j), 11(k), and 11(l)).

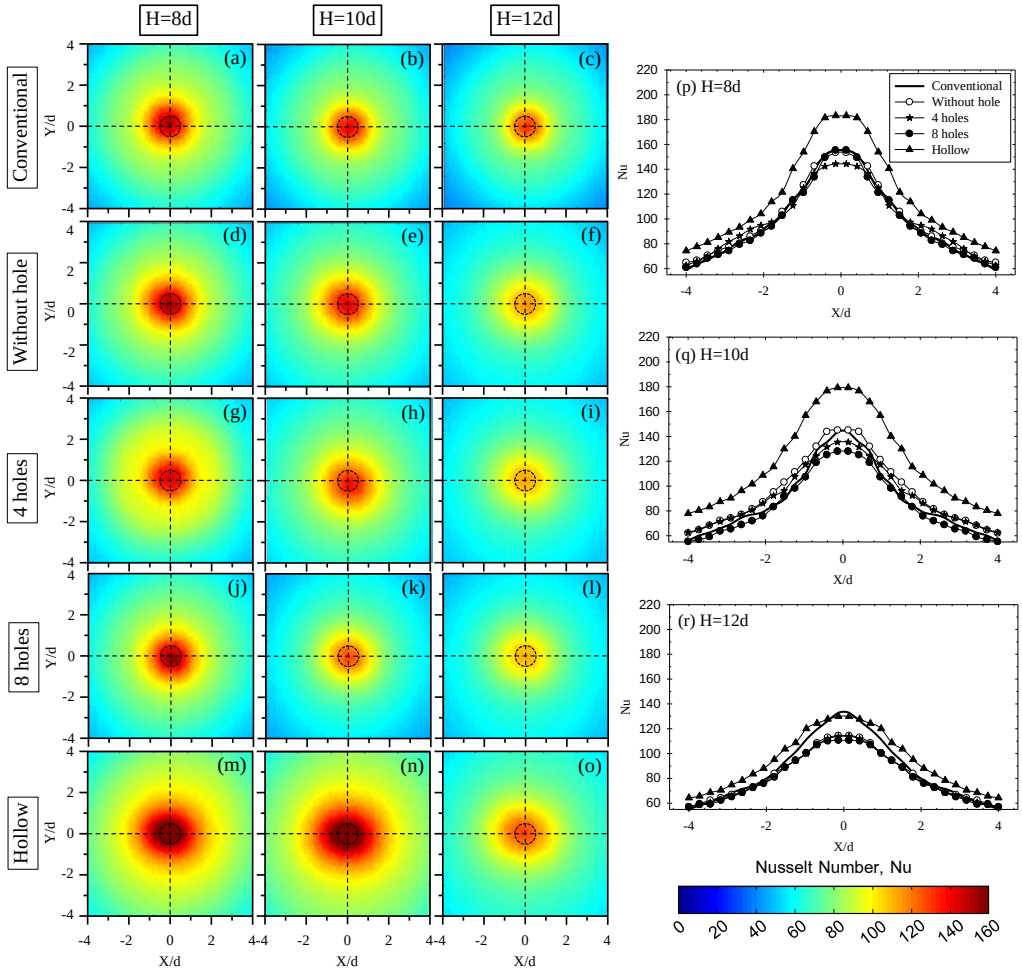

Figure 11 Nusselt number contours on impingement surface and comparison of Nusselt number distributions for the case of L=6d (Experimental result, Re=20,000)

For the hollow expansion pipe (Figure 9(m), 9(n), 9(o), Figure 10(m), 10(n), 10(o) and Figure 11(m), 11(n), and 11(o)), the Nusselt number distributions obviously increased higher than the other cases under the same conditions. Especially at the case of H=4d at L=2d as shown in Figure 9(m), the area of high Nusselt number was the largest due to high momentum of jet impinging on the surface which has been discussed in a previous section.

For the expansion pipe with 4 air entrainment holes, the circulation flow was introduced inside the expansion pipe and blocked the air flow from the air entrainment holes. This is the reason that the effect of drilling air entrainment holes cannot increase the heat transfer on the impingement surface compared with the case of expansion pipe without air entrainment holes and conventional pipe under the same conditions. Especially for case of 8 air entrainment holes, the heat transfer decreases. However, for the hollow expansion pipe, the increase of heat transfer is remarkable.

The heat transfer increasing of the jet from a hollow expansion pipe is exactly the same as the increasing entrainment air, especially entering of secondary entrainment air through hollow expansion pipe as discussed in previous section. Importantly, we show that heat transfer for the hollow expansion pipe is higher than that of the conventional pipe. The jet entrainment for the conventional pipe is mainly from primary entrainment air while the hollow expansion pipe is from both primary and secondary entrainment airs. Specifically, the secondary entrainment air is more effect on increasing the heat transfer on impingement surface.

Average Nusselt number calculated from average temperature in area of $0 \le r/d \le 4$ at Re=20,000 is shown in Figure 12. The average Nusselt number almost decreased corresponding to the decreasing of jet-to-plate distance (H) as well as expansion pipe length (L). The average values for the case of expansion pipe are almost higher than the conventional pipe. For the case of hollow expansion pipe, the average values are higher than the others throughout jet-to-plate distance (H) as well as expansion pipe length (L). The highest average values are took place for the case of hollow expansion pipe at L=2d and D=4d by getting higher 25.42% than the case of conventional impinging jet.

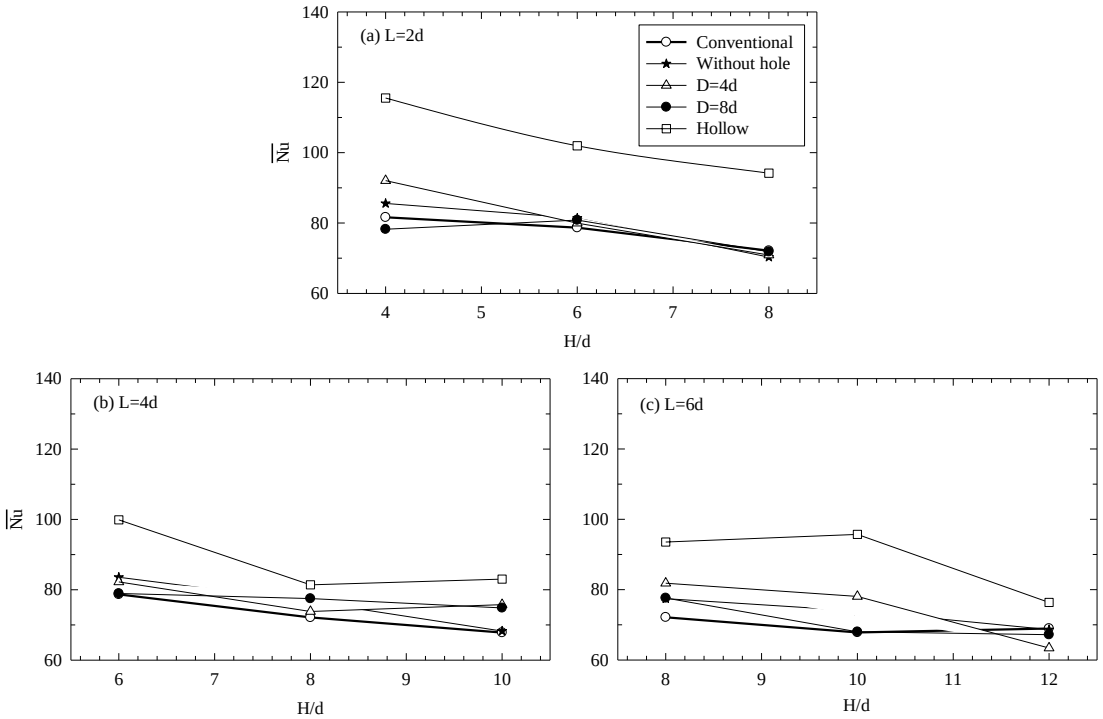

Figure 12 Average Nusselt number in area of $0 \le r/d \le 4$ (Experimental result, Re=20,000)

5. Conclusions

In this work, flow and heat transfer characteristics on the surface of an impinging jet from some modified expansion pipe were studied. To explore the condition of heat transfer augmentation on the surface, the expansion pipe without air entrainment holes, expansion pipe with 4 and 8 air entrainment holes, and hollow expansion pipe were considered. The results show that the heat transfer on the surface of an impinging jet with hollow an expansion pipe was higher than the other cases, especially for case of L=2d at H=2d. This condition can provide more air entrainment impinging on the surface. However, for the case of expansion pipe with air entrainment holes, the heat transfer on the surface is not different than the conventional pipe and expansion pipe without air entrainment holes due to internal blocking of circulation flow near the expansion pipe outlet. Especially for the case of 8 air entrainment holes, the heat transfer on the surface is the lowest.

6. Acknowledgements

This research was supported by The Faculty of Engineering and Postdoctoral Fellowship from Prince of Songkla University. The authors also gratefully acknowledge research funding from Prince of Songkla University (ENG540633s).

7. Nomenclatures

A	Area of heat transfer surface
d	Diameter of pipe nozzle
D	Diameter of air-augmented duct
h	Heat transfer coefficient
H	Pipe nozzle-to-impingement surface distance
I	Electrical current
k	Jet thermal conductivity
L	Length of air-augmented duct
Nu	Nusselt number
$\overline{Nu}$	Area-averaged Nusselt number
$\dot{q}$	Heat flux rate
Re	Reynolds number of jet
S	Distance from air-augmented duct outlet to surface
T	Temperature
$\overline{T}$	Average temperature
V	Electrical voltage

Greek symbols

ε	Emissive coefficient
σ	Stefan-Boltzmann constant

Subscripts

aw	Adiabatic wall (without heat flux)
input	Electrical power input
j	Jet
c	Natural convection
r	Radiation
s	Surrounding
w	Impingement wall, Wall with heat flux

8. References

Ashforth-Frost, S., & Jambunathan, K. (1996). Effect of nozzle geometry and semi-confinement on the potential core of a turbulent axisymmetric free jet. *International Communications in Heat and Mass Transfer*, *23*(2), 155-162. DOI:10.1016/0735-1933(96)00001-2

Ashforth-Frost, S., Jambunathan, K., & Whitney, C. F. (1997). Velocity and turbulence characteristics of a semi confined orthogonally impinging slot jet. *Experimental. Thermal and Fluid Science*, *14*(1), 60-67. DOI:10.1016/S0894-1777(96)00112-4

Baughn, J. W., & Shimizu, S. (1989). Heat transfer measurements from a surface with uniform heat flux and an impinging jet. *Journal of Heat Transfer*, *111*(4), 1096-1098. DOI:10.1115/1.3250776

Gao, N., Sun, H., & Ewing, D. (2003). Heat transfer to impinging round jets with triangular tabs. *International Journal of Heat and Mass Transfer*, *46*(14), 2557-2569. DOI:10.1016/S0017-9310(03)00034-6

Gulati, P., Katti, V., & Prabhu, S. V. (2009). Influence of the shape of the nozzle on local heat transfer distribution between smooth flat surface and impinging air jet. *International Journal of Thermal Sciences, 48(3)*, 602-617. DOI:10.1016/j.ijthermalsci.2008.05.002

Hasan, M. A. Z., & Hussain, A. K. M. F. (1982). The self-excited axisymmetric jet. *Journal of Fluid Mechanics*, *115*(2), 59-89. DOI:10.1017/S0022112082000652

Heo, M-W., Lee. K.-D., & Kim, K.-Y. (2011). Optimization of an inclined elliptic impinging jet with cross flow for enhancing heat transfer. *Heat and Mass Transfer*, *47*(6), 731-742. DOI:10.1007/s00231-011-0763-2

Martin, R. H., & Buchlin, J. M. (2011). Jet impingement heat transfer from lobed nozzles. *International Journal of Thermal Sciences*, *50*(7), 1199-1206. DOI:10.1016/j.ijthermalsci.2011.02.017

Huang, L., & El-Genk, M. S., (1998). Heat transfer and flow visualization experiments of swirling, multi-channel, and conventional impinging jets, *International Journal of Heat and Mass Transfer*, *41*(3), 583-600. DOI:10.1016/S0017-9310(97)00123-3

Katti, V., & Prabhu, S. V. (2008). Influence of spanwise pitch on local heat transfer distribution for in-line arrays of circular jets with spent air flow in two opposite directions. *Experimental Thermal and Fluid Science*, *33*(1), 84-95. DOI: 10.1016/j.expthermflusci.2008.07.004

Katti, V., & Prabhu, S. V. (2009). Influence of streamwise pitch on the local heat transfer characteristics for in-line arrays of circular jets with crossflow of spent air in one direction. *Heat and Mass Transfer*, *45*(9), 1167-1184. DOI: 10.1007/s00231-009-0491-z

Kline, S. J., & McClintock, F. A. (1953). Describing uncertainties in single-example experiments. *Mechanical Engineering*, *75*(1), 3-8.

Lytle, D., & Webb, B. W. (1994). Air jet impingement heat transfer at low nozzle-plate spacings. *Intrnational Journal of Heat and Mass Transfer*, *37*(12), 1687-1697. DOI:10.1016/0017-9310(94)90059-0

Nathan, G. J., Hill, S. J., & Luxton, R. E. (1998). An axisymmetric 'fluidic' nozzle to generate jet precession. *Journal of Fluid Mechanics*. *370*(1), 347-380. DOI:10.1017/S002211209800202X

Nathan, G. J., Alwahabi, M. J., Newbold, Z. T., & Nobes, D. S. (2006). Impacts of a jet's exit flow pattern on mixing and combustion performance. Progress in Energy and Combustion Science. 32(5-6), 496-538. DOI:10.1016/j.pecs.2006.07.002

Nuntadusit, C., Wae-hayee, M., Bunyajitradulya, A., & Eiamsa-ard, S. (2012). Heat transfer enhancement by multiple swirling impinging jets with twisted-tape swirl generators. *International Communications in Heat and Mass Transfer*, *39*(1), 102-107. DOI:10.1016/j.icheatmasstransfer.2011.10.003

Rohlfs, W., Haustein, H. D., Garbrecht, O., & Kneer, R. (2012). Insights into the local heat transfer of a submerged impinging jet: influence of local flow acceleration and vortex-wall interaction. *International Journal of Heat and Mass Transfer*, *55*(25-26), 7728-7736. DOI:10.1016/j.ijheatmasstransfer.2012.07.081

Salim, S. M., Ariff, M., & Cheah, S. C. (2010). Wall y+ strategy for dealing with wall-bounded turbulent flows, *Progress in Computational Fluid Dynamics. 10*(5-6), 341-351.

Selerowicz, W. C., Szumowski, A. P., & Meier, G. E. A. (1991). Self-excited compressible flow in a pipe-collar nozzle. *Journal of Fluid Mechanics*, *228*(7), 465-485. DOI: 10.1017/S0022112091002781

Viskanta, R. (1993). Heat transfer to impinging isothermal gas and flame jets. *Experimental Thermal and Fluid Science*, *6*(2), 111-134. DOI:10.1016/0894-1777(93)90022-B

Wae-Hayee, M., Tekasakul, P., Eiamsa-ard, S., & Nuntadusit, C. (2015). Flow and heat transfer characteristics of in-line impinging jets with cross-flow at short jet-to-plate distance. *Experimental Heat Transfer*, *28*(6), 511-530. DOI:10.1080/08916152.2014.913091

Zhou, D. W., & Lee, S.-J. (2004). Heat transfer enhancement of impinging jets using mesh screens. *International Journal of Heat and Mass Transfer*, *47*(10-11), 2097-2108. DOI:10.1016/j.ijheatmasstransfer.2003.12.002

Zuckerman, N., & Lior, N. (2006). Jet impingement heat transfer: physics, correlations, numerical modeling. *Advances in Heat Transfer*, *39*, 565-631. DOI:10.1016/S0065-2717(06)39006-5

Zeng, Y., New, T. H., & Tsai, H. M. (2009). On the use of notched collars on an axisymmetric jet. *Experimental Thermal and Fluid Science*, *33*(6), 1029-1034. DOI:10.1016/j.expthermflusci.2009.04.006

Zeng, Y., New, T. H., & Chng, T. L. (2011). Flow behavior of turbulent nozzle jets issuing from beveled collars. *Experimental Thermal and Fluid Science*, *35*(8), 1555-1564. DOI:10.1016/j.expthermflusci.2011.07.007